Research Papers

Performance assessment of phase change material-based thermal energy storage

Abhinav Rajan [a], Yixiang Gan [b], K.S. Reddy [a],[*]

[a] *Heat Transfer and Thermal Power Laboratory, Department of Mechanical Engineering, Indian Institute of Technology Madras, Chennai 600036, India*
[b] *School of Civil Engineering, The University of Sydney, NSW 2006, Sydney, Australia*

ABSTRACT

Phase change material (PCM) based thermal energy storage (TES) offers high energy density and better heat transfer performance by encapsulating PCM within a specifically designed container, i.e., shell and tube type TES. In this work, the PCM is packed in multiple cylindrical tubes, and heat transfer fluid (HTF) flows in the annulus. Such arrangement of PCM and HTF in the TES system is termed a cylindrical model, and the one opposite to the cylindrical model is called a pipe model. This work conducts the performance evaluation for PCM-based shell and tube TES using an experimentally validated numerical model. The 3D cyclic periodic model for TES has been developed based on hexagonal circle packing, and the effective energy storage ratio as a performance index under varying geometrical and operating parameters has been investigated. The variation in parameters includes tube length (0.5–7 m), diameter (10–50 mm), initial temperature (293.15–303.15 K), volumetric flow rate (10–500 l/min), inlet temperature (323.15–393.15 K). Using a conjugate heat transfer model, the influence of parameters was investigated, and the performance index was evaluated using the effectiveness-NTU theory. It was found that TES was effective for geometrical parameters diameter $d \leq 30$ mm and length $L \geq 2$ m. The performance index of 1.54 was optimum and achieved when the inlet temperature was 333.15 K. This optimum performance index value was compared with existing work and found to be performing comparatively well.

1. Introduction

The world has enormous dependencies on conventional energy sources, and meeting the demand for energy is a matter of concern with the depletion of traditional resources and its adverse impact on the ecosystem, i.e., carbon emission, climate, and global warming [1]. In this situation, renewable energy sources could be used as an alternative source to meet the energy requirement effectively and efficiently. Out of all renewable energy resources, solar energy grabs more attention worldwide because of its availability and high solar flux intensity. Different solar thermal technologies, such as flat plate, parabolic trough, and parabolic dish collectors, are used in heating and power generation at various operating temperatures [2]. Some applications are space heating/cooling [3] and industrial process heating [4]. The main challenge in utilizing the sun's energy is intermittent supply issues for various applications. To overcome intermittent supply issues, thermal energy storage (TES) can be a prominent way by integrating with solar thermal systems. Integrating TES improves the efficiency and

dispatchability of solar thermal technologies. Owing to their capability to absorb or release substantial latent heat, phase change material (PCM) based TES is generally gaining more attention than conventional TES [5]. Due to high energy density, easy operation, and affordability, latent heat TES is preferable for storage in different applications of all temperature operating ranges [6]. So far, the application of latent heat TES has not been explored well, and this machinery is in the research stage. Despite this, integrating TES (sensible and latent heat) with solar thermal technologies is quite visible in building heating applications, cold storage, solar water heating, etc. [7].

The shell-and-tube type of TES is frequently utilized in industrial and commercial applications. More than 70% of latent heat TES system studies involve shell-and-tube owing to its geometry and low heat loss [8]. It may be either pipe or cylindrical models [8]. In the pipe model, PCM is packed in the tube, and HTF flows in the annulus, whereas for the cylindrical model, HTF flows in a tube, and PCM is placed in the annulus. Based on shorter melting times, the pipe model was recommended rather than the cylindrical model [9]. Generally, cylindrical shell

---

geometry is considered so often due to its benefit in terms of heat transfer. The study was carried out with different geometrical containers filled with PCM and noticed that the time for storing the same amount of energy was least for cylindrical shell containers [10]. Moreover, studies on the effect of design parameters, including PCM and HTF properties and orientations, have been widely examined. The impact of orientation is experimentally observed for shell and tube TES using paraffin, and melting time decreased by approximately 30% with the inclination of 5° [11]. The charging rate was higher in horizontal than vertical orientations, while no evidence was noticed in the discharge process [12]. The cylindrical cascade system in a horizontal position took 13.33% shorter time to obtain 50% charging than a vertical orientation [13]. Further, the melting process using multiple PCMs with a fully turbulent flow was performed for the optimal length of each PCM in the horizontal direction [14]. The impact of HTF mass flow rate and temperature was extensively investigated for the phase change process [10–12,15,16]. Most studies were conducted on TES for the pipe model, and the cylindrical model has not been well explored.

Many studies have paid attention to increasing heat transfer in PCM to increase the viability of TES systems by achieving better thermal conductivity. Although PCM with higher energy density is valuable in improving TES performance, low thermal conductivity (0.2–0.5 W/m.K) [17] could lead to inefficiency for practical implementation on a large scale. In terms of increasing heat transfer, the best practice is mixing or encapsulating PCM with high thermal conductivity material. The graphite [18], metal foams (Ni, Cu, Al) [17], and carbon fillers [19,20] could increase effective thermal conductivity (20–50 times). It can notably improve the phase change rate, conditional to materials and their fractions. An alternative way to enhance heat transfer is by applying fins [21]. The longitudinal fins decreased the time of PCM melt and solidification by 24.52% and 43.6%, respectively [22], while for corrugated fins, time was reduced by 30–35% in solidification [23]. In the case of nano-enhanced PCM, longitudinal fins reduced the melting and solidification by around 54% and 76% compared to no-fin conditions [24]. Longer and thicker internal fins are recommended, and the effect of more fins is more noteworthy [25]. Other techniques to enhance heat transfer in PCM can be achieved using a multi-tube arrangement or providing eccentrics to the HTF tube in the shell. The melting time for PCM dropped remarkably by 53.3–71.1% when using four tubes in the shell, while in the case of finned four tubes, melting time was reduced by 65.78–83.33% than a single tube [26]. Besides, eccentric to the HTF tube in the shell of the TES also lowers the melting time of PCM. The melting time was 50.4% for an eccentricity factor of 0.5 compared to no-eccentric in the circular shell [27]. In the case of a triplex-type TES system, an eccentricity of +10 mm reduced melting time by 27.63% while a 12.82% reduction in solidification time for an eccentricity of 3 mm [28]. In recent practices, using fins with nanoparticles has increased for applications [29,30]. In a study [31], ceramic foam-enhanced molten salt in TES was used, and the small outer diameter with ceramic foam enhanced the performance with an improved storage rate of 54.9%. However, the total stored energy was decreased by 13.6% compared to the no-foam-filled case. Recently, molten salts, KNO_3, $NaNO_3$, and $NaNO_2$ in cascade shell and tube TES systems were investigated for high-temperature applications, and noticed cascade systems outperformed their single PCM counterparts during charging [32]. In the case of a packed bed TES system, the melting time for $NaNO_2$ was comparatively less than $NaNO_3$ [33].

Further, the performance and optimization of the TES system have been evaluated. The time for charging and discharging PCM is primarily used in calculating energy storage efficiency [9–11]. Based on the PCM melting time, geometrical design has been optimized numerically for different PCM materials [9]. In one study [34], the ratio of heat stored to mechanical energy consumption is proposed as the energy efficiency ratio. This ratio showed high sensitivity with tube diameter and decreased with increasing diameter and length. Another index to evaluate the performance of the latent heat TES system is the effective
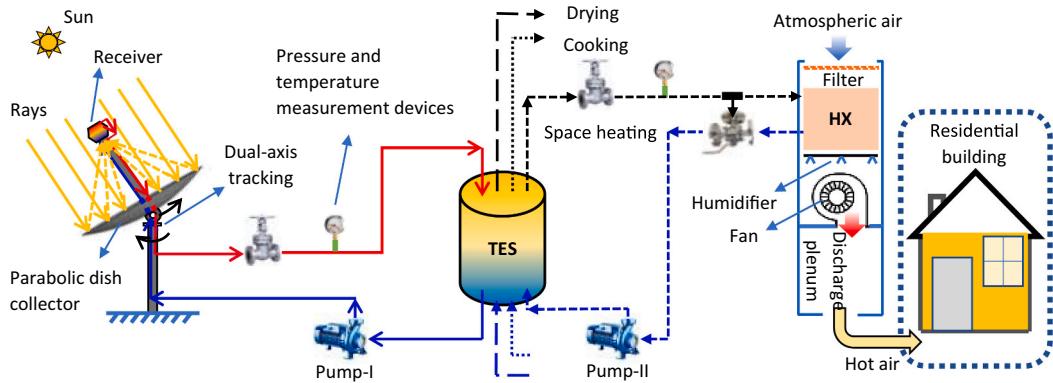
energy storage ratio [35], which is nothing but a ratio of stored heat by latent heat TES and conventional TES, i.e., an ideal stratified water storage. Based on this ratio, shell-and-tube TES performance has been optimized for NTU effectiveness of 0.8 in laminar and turbulent flow [36]. This ratio is proposed for the performance evaluation of TES in the present study. Moreover, the energy storage energy coefficient offered for maximizing the energy storage effect of the slab-type latent heat TES system considering the charging and discharge process and plate thickness in varying flow conditions [37]. In solar heating applications, a latent heat TES system is used with three different PCMs to evaluate the optimal number of tubes based on estimated thermal storage efficiency [38]. For the same applications, a comparison was made with the system without PCM, and based on the results proposed, implementing PCM does not signify the gain [39]. Also added, the design of the latent heat TES system is more fundamental to utilizing the intended potential of PCM to come true.

The present work proposes a performance evaluation to estimate the shell-and-tube TES system using the NTU method and formulation recommended by Fang et al. [35]. The shell-and-tube TES system is considered here, where pure PCM ($k = 0.2$ W/m.K) is packed in the multiple cylindrical tubes, and HTF surrounds it and flows in the annulus. The investigation on this TES model is not explored, while most studies were on the pipe model of the TES system. In the literature, as mentioned earlier, 2D modeling was reported. To build an accurate model, investigation using a 3D model is needed for the TES system. It was also noticed that very few works, as mentioned previously, were found for performance evaluation of the TES systems. In this view, the present study becomes essential in this field, and a 3D model has been built to perform the simulations. The performance index, i.e., effective energy storage ratio E_{st} has been evaluated numerically for the present TES model. This is the first attempt at performance evaluation of the current shell-and-tube TES cylindrical model. A 3D cyclic periodic model has been built for the TES system based on the hexagonal circle packing. The geometrical and operating parameters have been varied in this study to maximize the performance index. The variations in parameters, including tube length L, tube diameter d, initial temperature T_o, volume flow rate $\dot{V}$, and initial temperature T_i, are considered for the performance assessment of the shell-and-tube TES system. Furthermore, the optimized performance has been compared with other models. No such work has been carried out previously for the present model of the TES system.
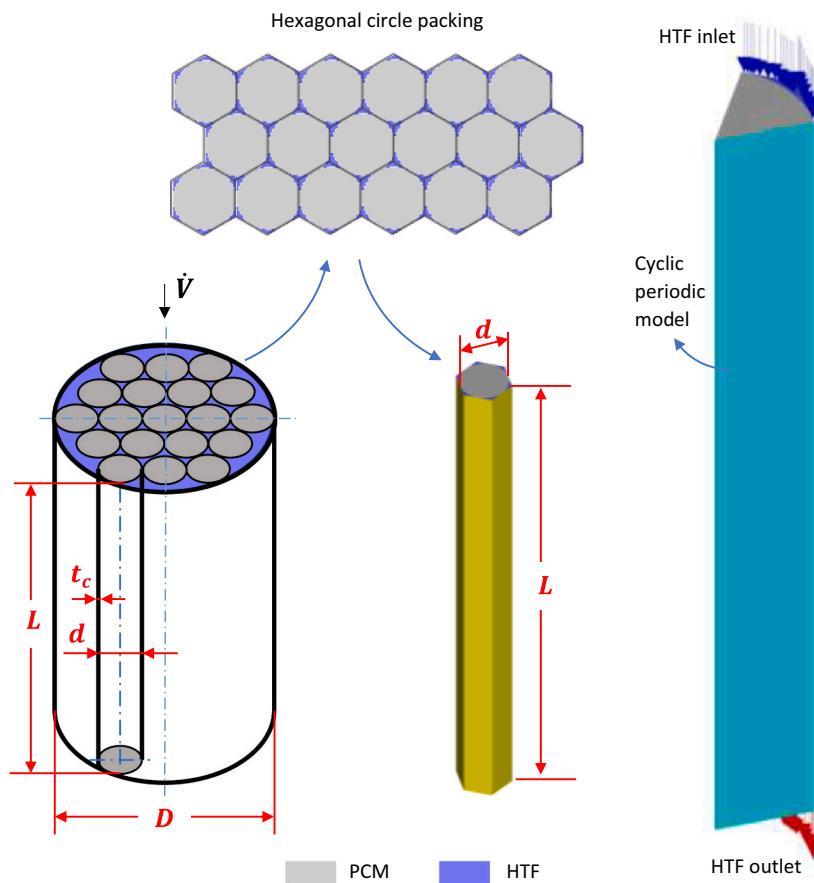
2. Methodology

2.1. System configuration

The PCM-based TES system stores and releases the heat during the phase change transition, offering a higher energy density and more efficiency than traditional storage systems [21,40]. This makes PCM-based TES systems helpful in storing thermal energy, which can be utilized in various applications, including integration with renewable energy systems [41,42]. One instance of an integrated solar energy system for process heating applications is shown in Fig. 1. The present study considers the shell and tube TES system where PCM is packed in the cylindrical tube, and HTF flows through the annulus. Such TES is a cylindrical model [8,9]. The hexagonal circle packing is assumed in the simulations [43]. In multiple PCM-packed cylindrical tube arrangements, only a single cylindrical unit was considered, with a hexagonal boundary around the PCM tube to consider the HTF in the annulus, as shown in Fig. 2. As the hexagonal domain is cyclic periodic, one-sixth (1/6) part of it is regarded as a computational domain in numerical modeling. By doing so, the computational expenditure could be reduced. The dimension of geometrical parameters for the TES system is provided in Table 1. For the considered range of investigating parameters (in Table 1), the diameter ratio satisfies $D/d \geq 10$ in this study.

Fig. 1. Integrated renewable energy system with thermal energy storage for cooking, drying, and space heating applications [41].

Fig. 2. Schematic of thermal energy storage, hexagonal circle packing assumption, and cyclic periodic model.

Table 1
Geometrical parameters in the study [36,43].

Parameter	Symbol	Value
Tank diameter (mm)	D	500
Tube length (m)	L	0.5–7
Tube diameter (mm)	d	10–50
Tube thickness (mm)	t_c	1

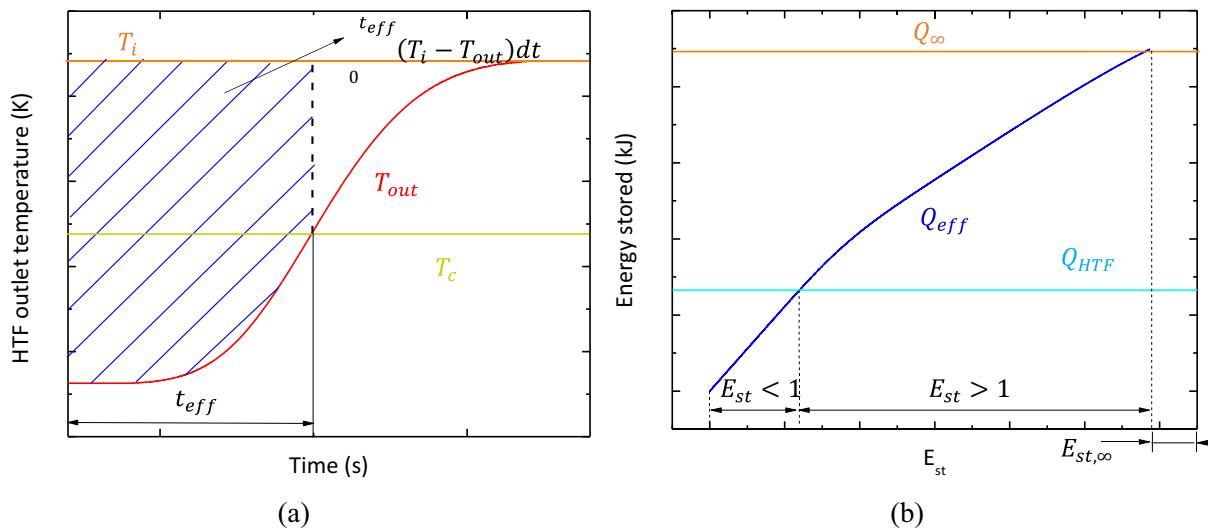Based on shell and tube TES, the performance index E_{st} for the melting PCM is specified as [35,36]:

$$E_{st} = \frac{Q_{eff}}{Q_{HTF}} \tag{1}$$

$$Q_{eff} = \int_0^{t_{eff}} \dot{m} c_{p,w} (T_i - T_{out}) dt \tag{2}$$

$$Q_{HTF} = \rho_w c_{p,w} V (T_i - T_o) \tag{3}$$

$$\dot{m} = \rho_w u_i A \tag{4}$$

where, Q_{eff} and Q_{HTF} are effective energy storage capacity of present TES and conventional water storage systems, respectively. t_{eff} is effective time and is defined as the time when HTF outlet temperature T_{out} reaches the specific value, i.e., cut-off temperature T_c. The pictorial representations for t_{eff} and temperature indices are shown in Fig. 3(a). $\dot{m}$ is mass flow rate, given by Eq. (4). The effective energy storage capacity

Fig. 3. Indices used in the study (a) estimation of performance index and (b) relations among the indices.

measures the actual stored heat in the TES unit during the melting process. V and T_o are volume and initial temperature, respectively. T_{out} is computed as the mass-weighted average of HTF outlet temperature and mathematically expressed as:

$$T_{out} = \frac{\int \rho u T dA}{\dot{m}} \tag{5}$$

where, ρ, u, T are the density, velocity, and temperature of the fluid. However, the HTF outlet temperature T_{out} was directly determined by taking the mass integral of temperature at the HTF outlet section in the Fluent solver.

The effective stored energy Q_{eff} is estimated before the HTF reaches a specific temperature value at the outlet. This particular value of HTF outlet temperature T_{out} is calculated via the NTU (number of transfer units) method. The NTU method has been frequently used to investigate the TES effectiveness of heat exchangers [44] and is expressed as the ratio of the actual to maximum heat transfer rate. For the TES system, it can be characterized as the ratio of the temperature difference across inlet and outlet sections to the maximum temperature change, as given in Eq. (6). In the charging process, PCM swaps the heat of HTF at phase change temperature, T_m (melting temperature of PCM) and T_m is used for estimating the maximum temperature difference.

$$\eta = \frac{T_i - T_{out}}{T_i - T_m} = 1 - e^{-NTU} \tag{6}$$

The melt temperature of PCM could be obtained as the average value of solidus and liquidus temperatures (T_s and T_l) of PCM.

$$T_m = \frac{T_s + T_l}{2} \tag{7}$$

where T_s and T_l are 317.2 K and 327.3 K for the PCM, respectively. The

Table 2
PCM properties in the modeling [45,46].

Property	Symbol	Value
Density (kg/m³)	ρ_{PCM}	820
Specific heat capacity (J/kg·K)	$c_{p.PCM}$	2000
Thermal conductivity (W/m·K)	k_{PCM}	0.2
Viscosity (kg/m·s)	μ_{PCM}	$5 \times 10^{-7} T^2 - 0.0004T + 0.0859$
Thermal expansion coefficient (1/K)	β_{PCM}	0.0006
Latent heat (J/kg)	L_h	170,320
Solidus temperature (K)	T_s	317.2
Liquidus temperature (K)	T_l	327.3

PCM properties in the study are provided in Table 2.

As per NTU, the effectiveness η drops with HTF outlet temperature rises. To guarantee the effective heat exchange between HTF and PCM, the least value of η must be evaluated for design optimization. In this study, the minimum value of 0.8 was selected for η. Thus, HTF outlet temperature corresponds to selected η should not go beyond a specific limit, which is termed the cut-off temperature T_c, to guarantee $\eta > 0.8$. The corresponding stored energy in the TES unit till $\eta > 0.8$ is evaluated as the effective energy storage capacity Q_{eff}. As mentioned above, supervising the HTF outlet temperature in the TES system ensures the effective exchange of heat between the HTF and PCM. Additionally, a direct need for outlet temperature may exist in applications. One such example is when releasing heat from the device in data centers and storing the same in TES, T_{out} must be under control under a specific value before it is sent back for cooling to prevent damage from excess temperature [43].

The performance of the present TES is decided by the effective energy storage ratio E_{st}, as defined in Eq. (1). When a latent heat thermal energy storage system, a TES unit using PCM, is not correctly designed, it could have an effective storage capacity significantly lower than the traditional or stratified water storage system. Therefore, constructing an effective PCM-based TES system for various influential parameters is essential and should perform better than a conventional storage system. This is how the performance of TES comes into play to signify whether a constructed PCM-based TES system is effective. If $E_{st} > 1$ implies that PCM-based TES is effective, indicating better energy-storing capacity than conventional TES systems. Or else, $E_{st} < 1$ shows ineffective compared to the conventional system. The schematic for calculating the performance index E_{st} and the used indices are illustrated in Fig. 3(b), where Q_∞ is theoretical energy storage capacity.

Based on the above considerations, the 3D numerical model has been developed for the present TES system. It is worth noting that most of the studies reported in the past were performed using a 2D model for TES systems where tube thickness t_c was not considered. Considering tube thickness t_c provides an understanding of actual conditions and improves accuracy in the results using a 3D model. The impact of tube thickness is provided in the Appendix. This study considers a tube thickness t_c of 1 mm [36].

2.2. Numerical model

The commercial finite volume method software ANSYS® 2020 R1 was adopted for numerical simulation. The conjugate heat transfer model includes fluid flow and heat transfer modulus used for simulating

PCM in the TES system. The enthalpy porosity method is used in ANSYS® Fluent 2020 R1 to simulate the solid-to-liquid phase shift. Natural convection is considered within the liquid PCM by enabling Boussinesq approximation. In the present work, the operating temperature is low, less than 373.15 K. Therefore, the Boussinesq approximation was suggested to perform flawlessly for natural convection by density variation under low operating temperatures [47]. In addition, it was used in PCM modeling in recent studies [32,46,48]. This approximation predicts well if changes in density are small. Mainly, the Boussinesq approximation is valid when $\beta(T - T_o) \ll 1$. In case of large temperature differences in the domain, the Boussinesq approximation should not be used [49].
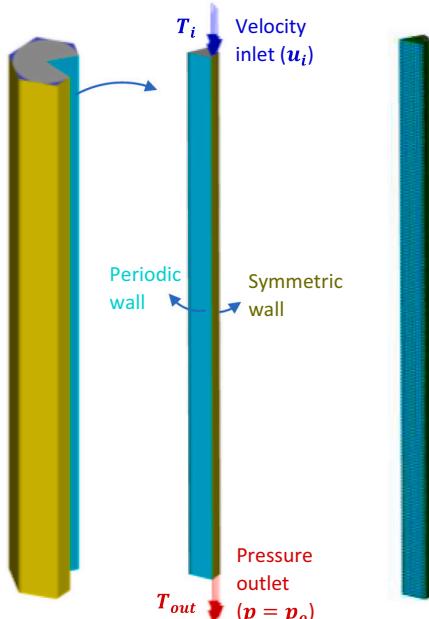
2.2.1. Assumptions in the modeling

Some pertinent assumptions have been made in this modeling as follows:

- Materials considered in modeling are homogeneous and isotropic in all phases.
- When melted, PCM pretends to be Newtonian fluid, and its flow is incompressible and laminar.
- The entire TES system is assumed to be at $T_o = 298.15$ K.
- Viscous dissipation and radiative heat transfer are ignored.
- Boussinesq assumption is included in the momentum equation that drives the natural convection.

2.2.2. Computational domain

As discussed earlier, the reduced computational domain, i.e., one-sixth part of the TES system, is considered in this study. The modeling uses a three-dimensional computational environment of one-sixth of the TES system. The computational domain with boundary conditions and mesh are provided in Fig. 4. The periodic wall conditions eliminate the need to model the entire single unit of hexagonal packing. This is how the computational cost for conducting the simulations is reduced. One hexagonal pack is symmetrical to each other, so the symmetric wall condition is defined at the hexagonal side of the domain.

Fig. 4. Computational domain with boundary conditions and grid generation.

2.2.3. Governing equation

The numerical model involves fluid flow and heat transfer methods to simulate the present cyclic model of a PCM-based TES system, investigates the charging process, and solves the governing equations in sequential order. The governing equations include continuity, momentum, and thermal equations and are given as follows [49]:

Continuity equation:

$$\nabla \bullet \vec{V} = 0 \tag{8}$$

Momentum equation:

$$\frac{\partial \vec{V}}{\partial t} + \vec{V} \bullet \nabla \vec{V} = \frac{1}{\rho} \left\{ -\nabla p + \mu \nabla^2 \vec{V} + \rho \beta \vec{g}(T - T_o) \right\} + \vec{S} \tag{9}$$

where, the term $\rho \beta \vec{g}(T - T_o)$ is the buoyant force that gives rise to natural convection in the liquid PCM through the Boussinesq approximation and $\vec{S}$ is Darcy's law damping source term. Due to the density difference between the solid and liquid phases, the buoyancy forces initiate natural convection currents. The convection currents intensify as more PCM transitions to the liquid phase. The evolution of natural convection in the PCM can be seen in Fig. 5. Further, $\vec{S}$ term in the momentum equation includes phase change effects on the heat transfer owned by convection. The source term, $\vec{S}$, is described as:

$$\vec{S} = \frac{(1 - \lambda)^2}{\lambda^3} A_m \vec{V} \tag{10}$$

where, A_m is a mushy zone constant. The value for this constant usually is 10^4–10^7. In the present investigation, a value of 10^5 is assumed for A_m based on model validation. λ is the melt fraction and is expressed as:

$$\lambda = \begin{cases} \dfrac{\Delta H}{L_h} = 0 \text{ if } T < T_s \\[2mm] \dfrac{\Delta H}{L_h} = 1 \text{ if } T > T_l \\[2mm] \dfrac{\Delta H}{L_h} = \dfrac{T - T_s}{T_l - T_s} \text{ if } T_s < T < T_l \end{cases} \tag{11}$$

Thermal energy [49]:

$$\rho \frac{\partial H}{\partial t} + \nabla \bullet \left(\rho \vec{V} H \right) = \nabla \bullet (k \nabla T) \tag{12}$$

The aggregate of sensible enthalpy and latent heat is estimated as the total enthalpy of the material.
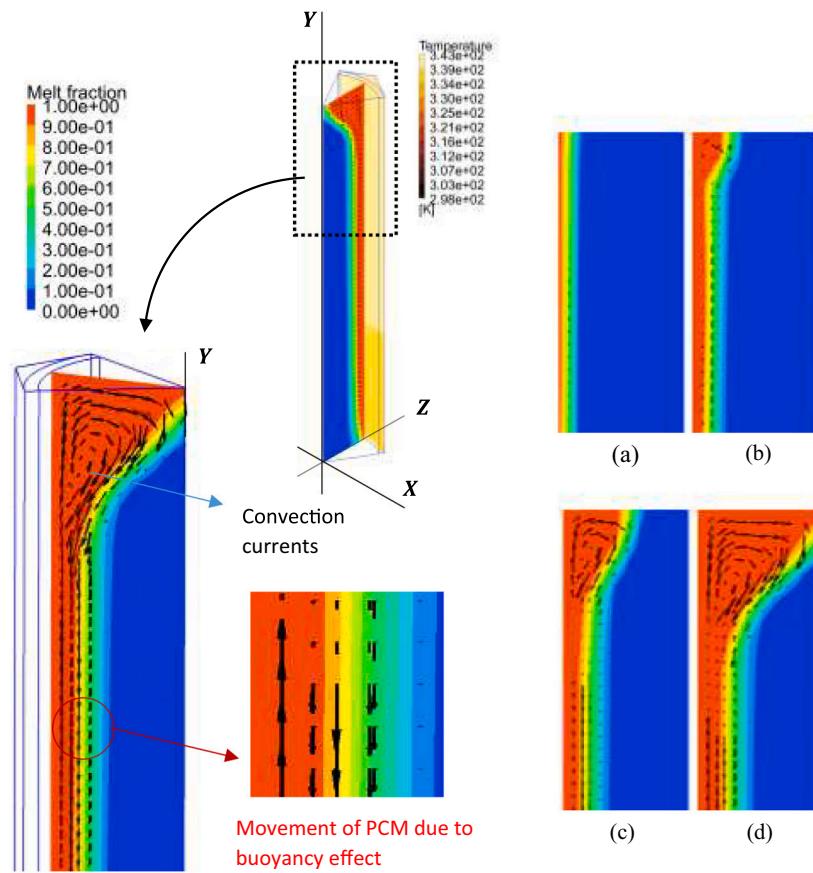
$$H = h_s + \Delta H \tag{13}$$

where,

$$h_s = h_{ref} + \int_{T_o}^{T} c_p \Delta T \tag{14}$$

The latent heat content can be defined as:

$$\Delta H = \sum_{i=1}^{n} \lambda L_h \tag{15}$$

where ΔH varies from 0 (solid) to L_h (liquid) and L_h is the latent heat of PCM.

The cyclic periodic model of the PCM-based TES system was built in ANSYS® Fluent 2020 R1. The Solidification and Melting model were
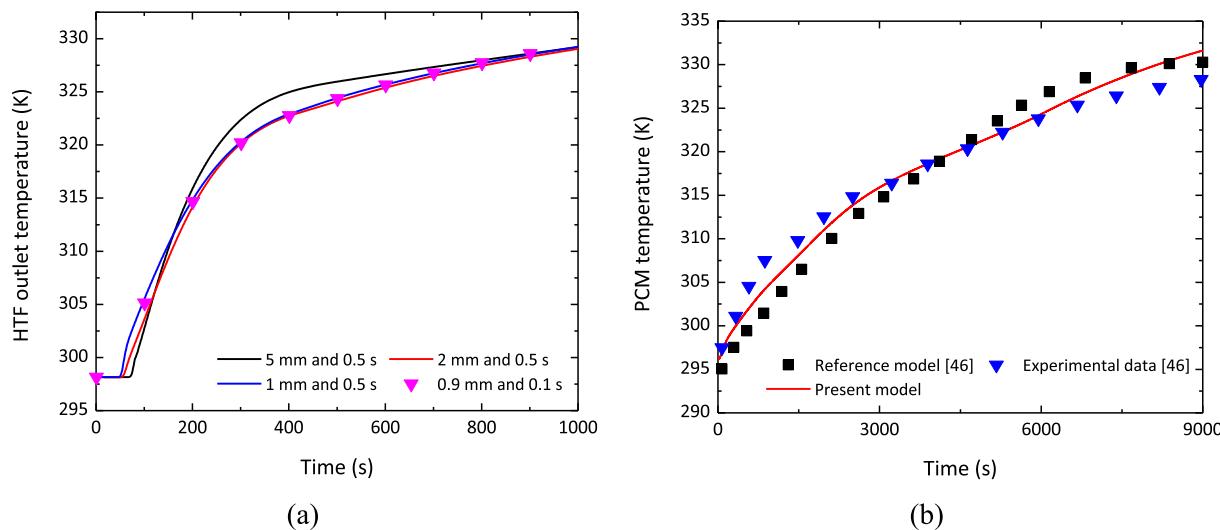
Fig. 5. Evolution of natural convection in the PCM (a) 60 s, (b) 120 s, (c) 180 s and (d) 240 s.

turned on for the phase change process in PCM while based on *Re* calculated from the corresponding volumetric flow rate $\dot{V}$, laminar was adopted as a flow model. The SIMPLE scheme was employed for pressure-velocity coupling and PRESTO! for pressure correction. The discretization for the rest of the equations was done using QUICK. The residuals of 10^{-4}, 10^{-4}, and 10^{-6} were set for continuity, momentum, and energy equations, respectively.

2.2.4. Initial and boundary conditions

HTF at 343.15 K was supplied at the entrance of the inlet section of the computational domain with a velocity u_i corresponding to the total volumetric flow rate $\dot{V}$ of 20 l/min. The HTF exits at atmospheric pressure from the outlet. The initialization of all configurations was done at 298.15 K. The lateral surface of the hexagonal side of the domain was symmetric; other than these, walls (side walls) were assumed to be

Fig. 6. (a) Grid and time independence test, and (b) model validation.

cyclic periodic walls, as shown previously in Fig. 4. The tube walls are defined as a no-slip condition, and thermal contact resistance and heat transfer at line contact among the tubes in the study were ignored.

2.2.5. Grid test and time independence test

The structured grid was generated to simulate the cyclic periodic model of the PCM-based TES system, as illustrated earlier in Fig. 4. The grid and time step sensitivity are essential to ensure the exactness of results with the computational expense. For this purpose, the cyclic periodic model ($d = 20$ mm and $L = 2$ m) was chosen. Here, the grid sensitivity test was conducted by progressively lowering the element size from 5 mm to 0.9 mm and computing T_{out}. The mesh counts varied from $2.0E+04$ to $1.46E+06$. Also, the time step independence study was carried out for 0.5 s and 0.1 s. It is noted that the element size and time step are reduced, and the HTF outlet temperature varies at first and then stabilizes. Fig. 6(a) illustrates the deviation in HTF outlet temperature for various element sizes at 0.5 and 0.1 s. Considering this, the optimum element size for the present cyclic periodic model of the PCM-based TES system is 1 mm at 0.5 s.

2.2.6. Model validation

A numerical model based on the experiment and numerical studies of Hosseini et al. [46] was developed to ensure the present conjugate model reliability in the study. The shell and tube configuration, dimensions given in Table 3, was modeled to build the numerical model as per Hosseini et al. [46]. The mesh and time step independence were ensured for validation. The element size and time step were taken as 2 mm and 1 s in the validation, respectively. The HTF and PCM were initially at 298.15 K, and the inlet was defined with a mass flow rate of 0.0167 kg/s at 343.15 K. The Paraffin wax (RT 50) was selected as PCM, and the properties are provided in Table 2. The average volume temperature of PCM over time was recorded and compared against the Hosseini et al. [46], as displayed in Fig. 6(b). It is evident in Fig. 6(b) that this model can predict the phase change process appropriately. The result from the present model lies between the reported numerical and experimental results of Hosseini et al. [46]. The deviation in results may be caused by differences in operating conditions and thermophysical properties of HTF and PCM used in the study. The present model agrees with the reported data and is expected to be reliable in the current modeling.

2.2.7. The setting of parametric studies

The initial condition intended to assess the effect of geometrical and operating parameters, including tube length L, diameter d, initial temperature T_o, volume flow rate $\dot{V}$ and inlet temperature T_i, is as follows: Initially, the whole TES system, including HTF and PCM, was maintained at 298.15 K. The volumetric flow rate $\dot{V}$ to TES was 20 l/min, so was 0.0182 m/s as calculated inlet velocity u_i for HTF (see Appendix). The inlet HTF temperature T_i was set at 343.15 K. The Paraffin wax (RT 50) as PCM was considered for low-temperature applications of TES, such as space heating. It is highly used organic PCM in TES for commercial applications due to its chemical stability, non-corrosive, non-toxic, and readily available in nature [50]. The properties of the present PCM are tabulated in Table 2. The melting temperature scale was set as $\Delta T = 10$ K for PCM. Further, for HTF, the default properties from the in-built material of liquid water in ANSYS® Fluent 2020 R1 were

Table 4
HTF properties considered from the in-built Fluent material database [49].

Property	Symbol	Value
Density (kg/m^3)	ρ_w	998.2
Specific heat capacity (J/kg·K)	$c_{p,w}$	4182
Thermal conductivity (W/m·K)	k_w	0.6
Viscosity (kg/m·s)	μ_w	0.001003

employed, provided in Table 4.

The effectiveness η of 0.8 was chosen as the minimum for the TES system, and as per this, the outlet temperature was decided as $T_{out} = 326.43$ K. In other words, the simulation would stop once the HTF achieved this temperature. The Table of Design Points settings in ANSYS® were used to create essential files and were uploaded to the High-Performance Computing Environment (HPCE, IIT Madras) for the numerical simulations. The range of investigating parameters is listed in Table 5.

The TES configuration of $L = 2$ m and $d = 20$ mm was selected to carry out the independence study on grid and time step and reported HTF outlet temperature in the previous section. Based on this study, the mesh element size and time step were chosen as 1 mm and 0.5 s for all simulations.

3. Results and discussion

3.1. Variation of length (L)

The tube length from 0.5 m to 7 m was taken in the study. The tube diameter was set as $d = 20$ mm for pure PCM (0.2 W/m.K). The influence of length L on the HTF outlet temperature and performance index E_{st} are presented in Fig. 7(a, b).

Fig. 7(a) exhibits the variation of HTF outlet temperature over time for increasing length of the tube till the T_{out} reach the cut-off temperature ($T_c = 326.43$ K). It can be noticed in Fig. 7(a) that the time for reaching T_c increases with length. As clear, a more considerable tube length accommodates more PCM volume, which needs more time for melting the PCM with heat exchange with HTF. While for shorter tube lengths, melting proceeds very quickly, and the HTF outlet temperature reaches T_c comparatively in less charging time compared to longer-length tubes. Noticed that the trends of the curve are regular, except for a higher tube length, say greater than 4 m. For the said lengths, temperature variation is almost negligible for around 2000–4000 s, and curves seem flat over a short period. This is so happening due to the phase transition of PCM ($T_s = 317.2$ K), and a high volume of PCM with length requires more phase transition time. For shorter lengths, the phase transition happens very swiftly due to low PCM volume, and the transition is not even noticeable. Nevertheless, it appears with the further increase in length. It is also noticed that the HTF outlet temperature T_{out} with increasing length is not varied. Based on a study of PCM-based TES units, in the solid phase, the HTF outlet temperature T_{out} increases because the energy that is being transferred from HTF to PCM becomes lower over time. On the same principle as in the solid phase, during the liquid phase of the PCM, the HTF outlet temperature T_{out}
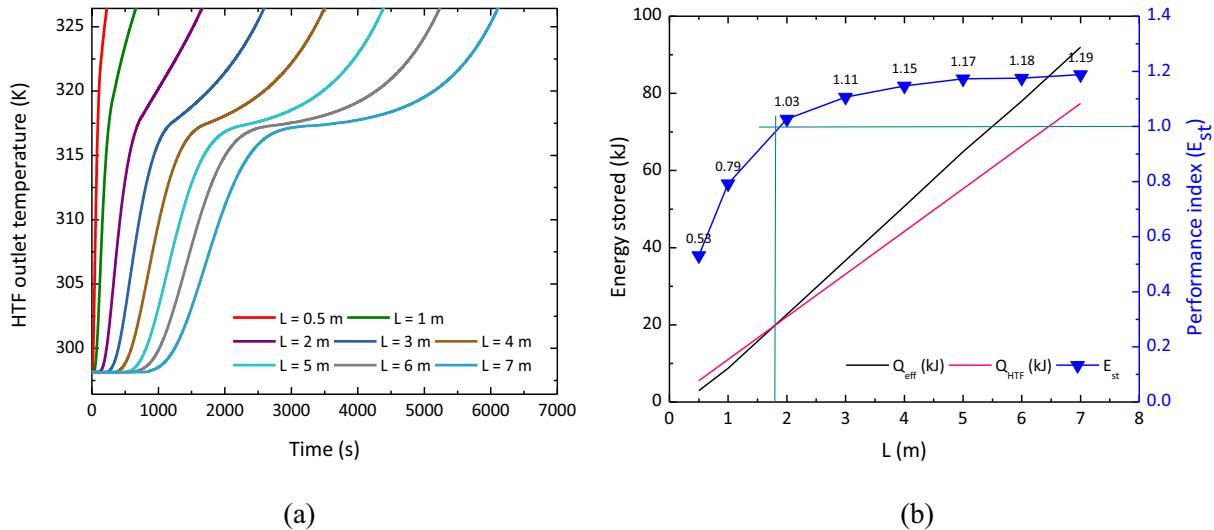
Table 3
Geometrical details for model validation [46].

Parameter	Value
Tube length (m)	1
Outer diameter (mm)	85
Inner diameter (mm)	22
Tube thickness (mm)	2.5

Table 5
Range of the investigated parameters in the study.

Parameter	Symbol	Value
Length (m)	L	0.5–7
Tube diameter (mm)	d	10–50
Initial temperature (K)	T_o	293.15–303.15
Volumetric flow rate (l/min)	$\dot{V}$	10–500
Inlet temperature (K)	T_i	323.15–393.15

Fig. 7. Variation of tube length for $\dot{V}$ = 20 l/min, k = 0.2 W/m.K (a) HTF outlet temperature, and (b) effective energy storage and performance index.

increases [51]. Therefore, if the outlet temperature of the heat transfer fluid is not changing, it is possible that all the heat is being absorbed by the PCM in the TES system and is transferred axially in the PCM over time. This is so confirmed by the temperature distribution, as illustrated in Fig. 8. The temperature contours at the outlet (y/L = 1) show no variation till 180 s, further change can be noticed for 360 s. The effective stored energy and performance index are evaluated for the length variation mentioned above and reported in (b). It can be viewed in Fig. 7 (b) that with the increasing tube length, the performance index (E_{st}) increases. This implies that the TES system performs better with the longer tubes. The increase in E_{st} may be instigated by complex heat transfer of PCM and HTF.

It should be noted that $E_{st} < 1$ for $L < 2$ m, which means that TES would be ineffective. When TES is effective, i.e., $E_{st} > 1$ as the tube length increases, the performance index increases, indicating an effective TES system. The improve in E_{st} for length from 2 m to 5 m is 15%, and further, there is marginal variation in E_{st}. It means that the increasing tube length after 5 m will not add much impact on increasing E_{st}, since the increasing speed of E_{st} slows down.

The melt fraction and temperature contours of L = 2 m for complete melting of PCM are shown in Fig. 8. Also, the temperature distribution for HTF and PCM is shown in Fig. 9. These temperature distributions show the variation in the axial direction with increasing time from 0 s to 2910 s. The temperature of both HTF and PCM increases with increasing time. In the meantime, the rise rate of the temperature of PCM is lesser than that of HTF. Once the charging is done, the HTF and PCM in the TES tank achieve the inlet temperature T_i, which indicates no further heat exchange and effective energy storage, as per Eq. (2).

The previous results showed the advantage of having longer tubes in a shell-and-tube TES system in terms of performance index E_{st}. Conversely, concerning the pump with increasing tube length L, there would be high-pressure drop and energy consumption. Thus, energy consumption caused by the pressure loss needs to be considered. Taking only major losses in the flow into account, the energy consumption would be given as for the pump [52]:

$$Q_{pump} = \Delta p \dot{V} t = \left(\rho \frac{64}{Re} \frac{L}{d_h} \frac{\bar{u}}{2} \right) \dot{V} t \qquad (16)$$

The ratio Q_{pump}/Q_{eff} in percentage variation with length L, signifying the fraction of pump energy consumption in Q_{eff}. Fig. 10(a) shows that with tube length, the percentage increases marginally. The percentage increase appears to be linear with tube length. It can be seen in Fig. 10(a)

that the pump energy consumption Q_{pump} is negligible when compared with effective energy storage Q_{eff}. Liang et al. [36] also reported the pump energy consumption was marginal compared to Q_{eff} and considered it negligible.

In the meantime, the production energy as length increases also increases. The total primary energy consumed for producing materials is termed embodied energy [53] and is applicable to be measured for the TES system. The Copper tube was considered to have a thickness t_c of 1 mm and a density of 8978 kg/m³ in the study. The average embodied energy for a Cu tube (50% recycled) was picked as 55 MJ/kg [53], and for a specific length of the tube, embodied energy $Q_{embodied}$ was evaluated. Then, the energy payback cycle could be described by Eq. (17).

$$\eta_{cycle} = \frac{Q_{embodied}}{Q_{eff}} \qquad (17)$$

The energy payback cycle η_{cycle} is illustrated in Fig. 10(b) for varying lengths. As length increases, the energy payback cycle decreases. It means that energy investment in the material can be paid off earlier for longer tubes in the TES system. The energy payback cycle η_{cycle} reduces abruptly once changed the tube length L from 0.5 m to 3 m, and no substantial change in η_{cycle} further. Therefore, minimum value of length for tubes must be confirmed for an appropriate small-energy payback cycle η_{cycle} [36]. As conclusion, believing negligible energy consumption of the pump compared to energy stored in TES, longer tube length is always considered to be perfect for progressing system performance in terms of both performance index E_{st} and energy payback cycle η_{cycle}. This statement aligns with the literature [36]. Based on estimated performance E_{st} and energy payback cycle η_{cycle}, the tube length L of 5 m has been considered in the further simulations.

3.2. Variation of diameter (d)

In the present TES system, the PCM is packed in a cylindrical tube, and in the annulus, HTF flows, as schematically shown previously. Here, the variation in tube diameter not only varies PCM volume but also changes flow conditions in HTF. Due to this, the variation in tube diameter is worth examining. To inspect the tube diameter effect, the parametric cases with varying d from 10 mm to 50 mm were conducted. The thermal conductivity was set as k = 0.2 W/m.K (pure PCM). The length of the tube, L was fixed at 5 m. The inlet velocity u_i was 0.0182 m/s. The effect of tube diameter on HTF outlet temperature is shown in
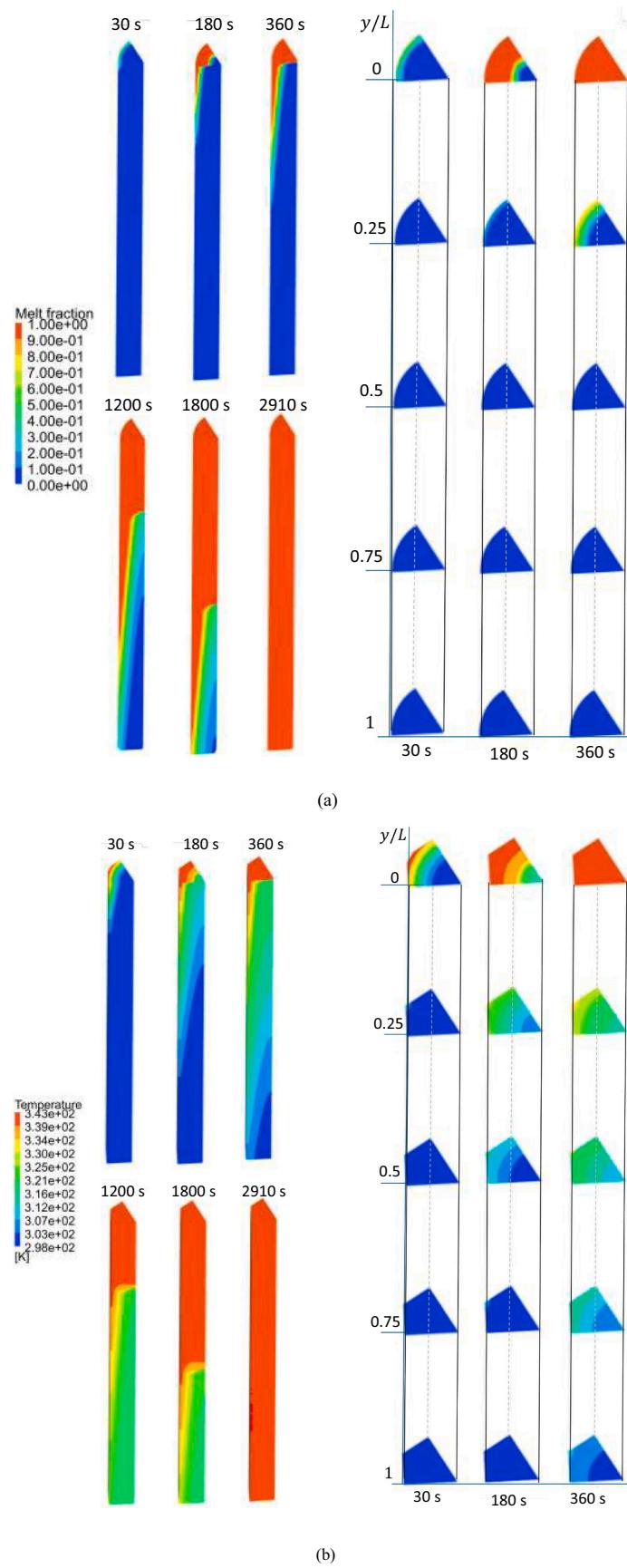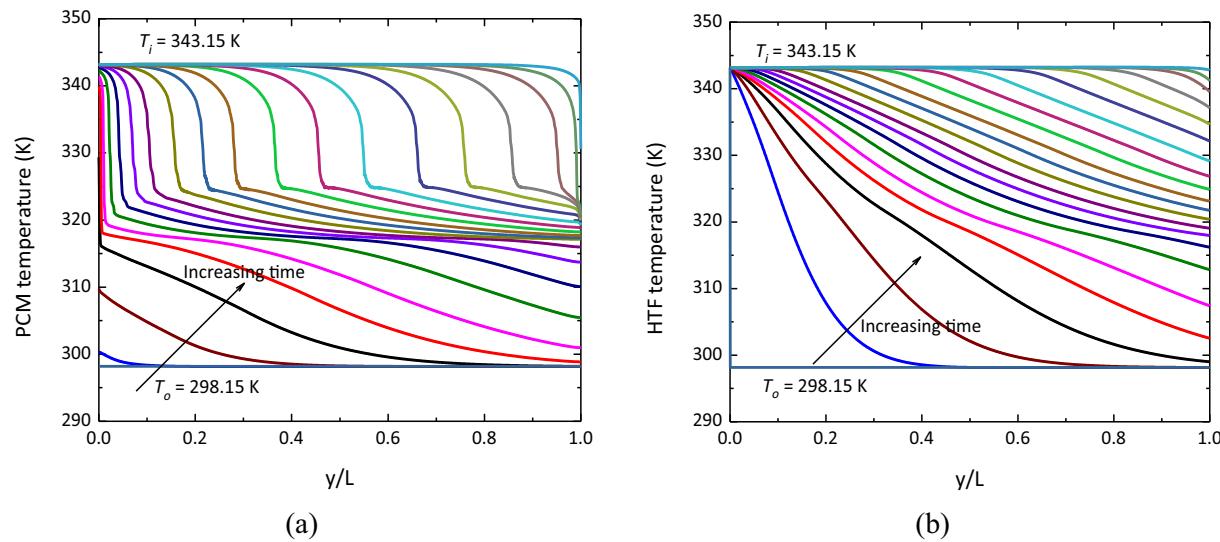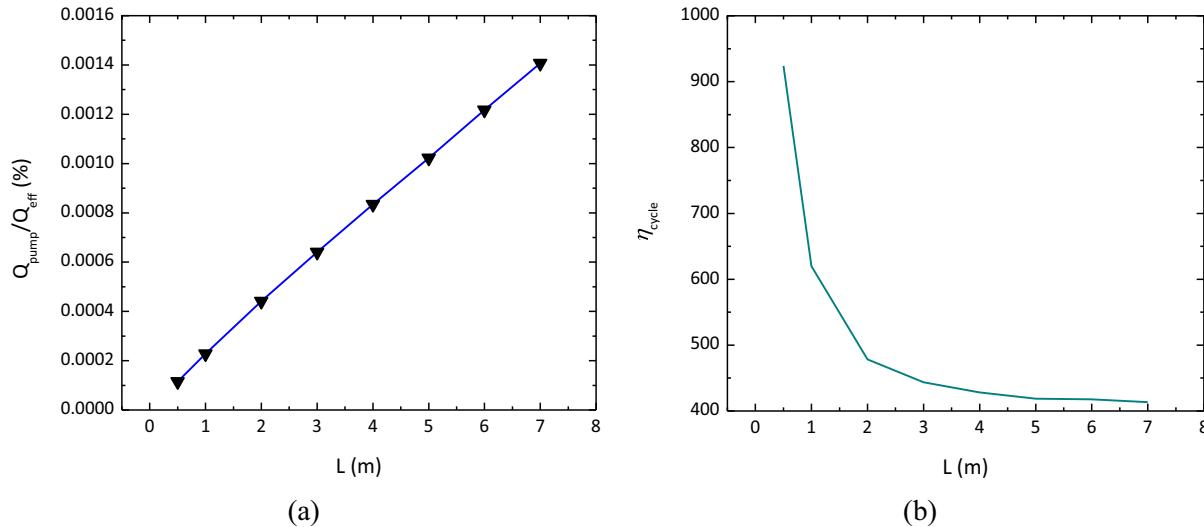
(a)

(b)

Fig. 8. Contours for L = 2 m (a) melt fraction of PCM (b) temperature contours of PCM and HTF.

Fig. 9. Temperature distribution in axial direction (a) PCM and (b) HTF.

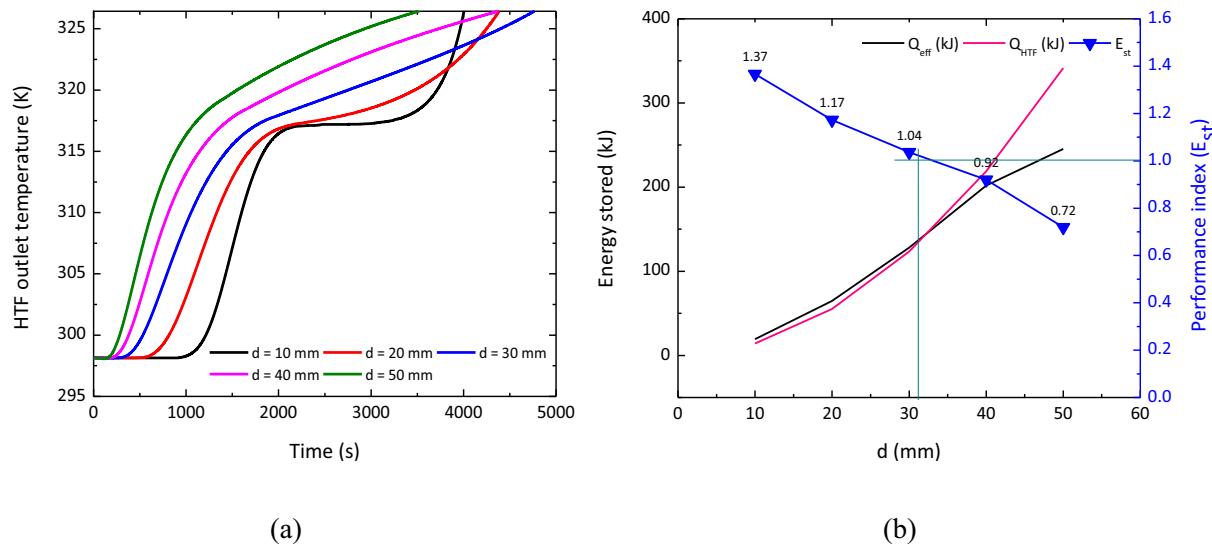**Fig. 10.** (a) The proportion of Q_{pump} in Q_{eff} versue L, and (b) energy payback cycle versus L.

Fig. 11(a, b).

Fig. 11(a) presents that as tube diameter reduces, the time when T_{out} attains 326.43 K increased. The trend of curves for d = 30 to 50 mm is quite similar. For $d \leq 20$, the trends are more wavey over the time. The phase transition is noticed for smaller tube diameters up to 20 mm. Here, the fact is that the HTF flow area is reduced with decreasing tube diameter, which slows down the mass flow rate of HTF. The melting of PCM with a slower mass flow rate requires more time for the phase transition, which is why the curve shows no variation in temperature for the phase transition period. The performance index E_{st} is evaluated which is ratio of Q_{eff} and Q_{HTF}, and shown in Fig. 11(b). It is noticed that E_{st} decreases with increasing d. The increase in d incorporates more PCM volume and increases the HTF flow area hence mass flow rate. The fact behind decreasing E_{st} with increase in d is that the mass flow rate is more dominating with increasing d due to which time when T_{out} reaches certain value decreases and heat exchange drops significantly between HTF and PCM. When $E_{st} > 1$, it indicates a more effective TES system. It is noticed that TES is effective for d up to 30 mm. Therefore, tubes with
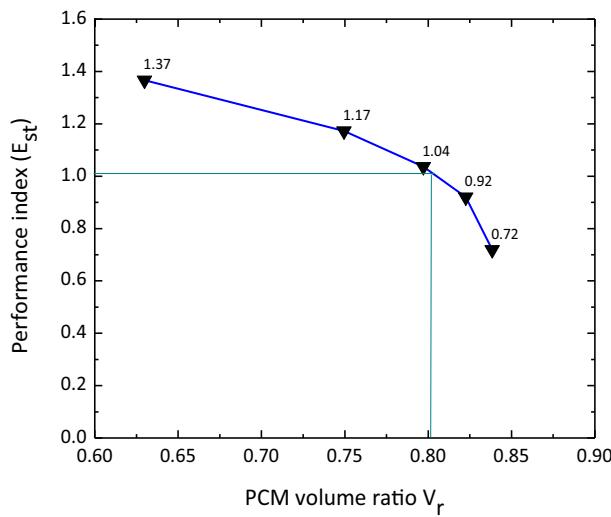
smaller diameter are beneficial to energy storage effectiveness for the present TES system. Further, The PCM volume ratio V_r varies with changing d, so plot for V_r versus E_{st} is shown in Fig. 12. The PCM volume ratio V_r is outlined as the fraction of PCM volume to volume to entire TES system. The trend of E_{st} against V_r is of decreasing in nature, while Liang et al. [36] reported it as increasing. Here it can be noted that Linag et al. [36] heated the PCM by putting an internal HTF tube in it, while in the present work, heating PCM is done externally. In external heating, the increase in V_r as d increases adds up more PCM layers with high mass flow rate, and the thermal resistance dominates that yields in lowering E_{st}. It should be noticed that TES system would be effective for V_r up to 0.8. Beyond 0.8, the heat exchange between the PCM and HTF hinders and shows TES system ineffective.
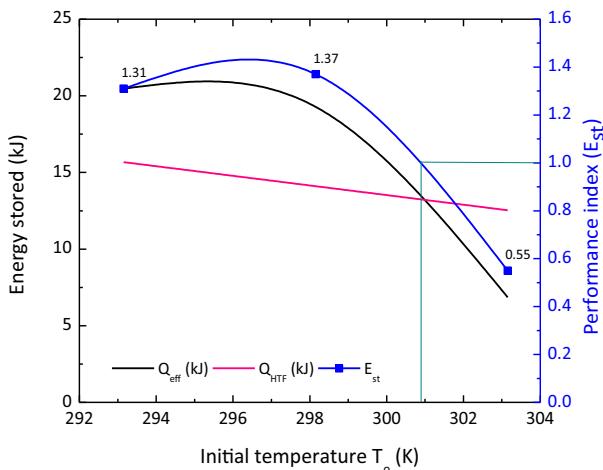
3.3. Variation of initial temperature (T_o)

A temperature range from 293.15 to 303.15 K was taken to investigate the impact of initial temperature T_o. The tube diameter and length
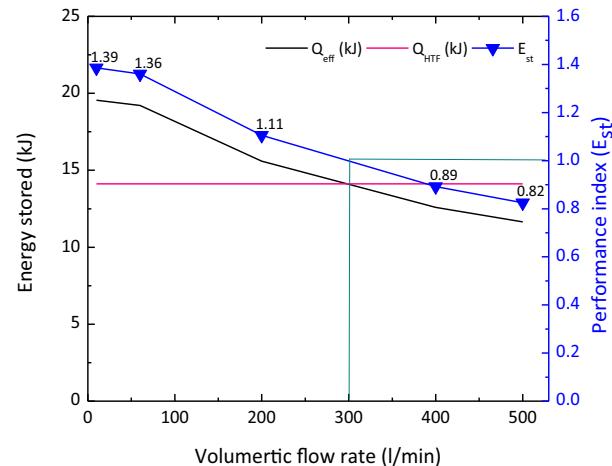
Fig. 11. Effect of tube diameter for $\dot{V} = 20$ l/min, $k = 0.2$ W/m.K (a) HTF outlet temperature, and (b) effective energy storage and performance index.

Fig. 12. PCM volume ratio versus E_{st}.

Fig. 13. Effect of initial temperature (T_o) on stored energy and performance index.

Fig. 14. Volumetric flow rate ($\dot{V}$) versus stored energy and performance index.

were set as $d = 10$ mm and $L = 5$ m. The influence of initial temperature T_o on energy stored and performance index is shown in Fig. 13. It is noticed that with increasing initial temperature of the TES system, Q_{eff} decreases and consequently E_{st}. The increase in E_{st} for T_o from 293.15 K to 298.15 K was about 5% and for a further 60% drop in E_{st} for T_o from 298.15 K to 303.15 K. For T_o from 293.15 K to 298.15 K, Q_{eff} decrease by only 5% while Q_{HTF} by 10%, so is its ratio (E_{st}) increased by 4.5%. Further, it is noticed that with increasing initial temperature, the temperature difference ($T_{in} - T_o$) in Q_{HTF} decreases, but effective energy store (Q_{eff}) reduced by greater extent. As a result, the ratio of Q_{eff} and Q_{HTF} significantly decreases hence so is E_{st}. The $E_{st} > 1$ for $T_o < 301$ K, the TES system would be effective for lower T_o.

3.4. Variation of volumetric flow rate ($\dot{V}$)

The volumetric flow rate to the TES system is one of the factors on which performance depends and is worth exploring. To inspect the volumetric flow rate $\dot{V}$, parametric cases with $d = 10$ mm and $L = 5$ m were conducted for pure PCM. The calculated inlet velocity u_i corresponding to $\dot{V}$ varied from 10 l/min to 500 l/min was defined in the simulations with $T_i = 343.15$ K. The stored energy and performance index E_{st} are shown in Fig. 14. It is noticed that the effective energy store
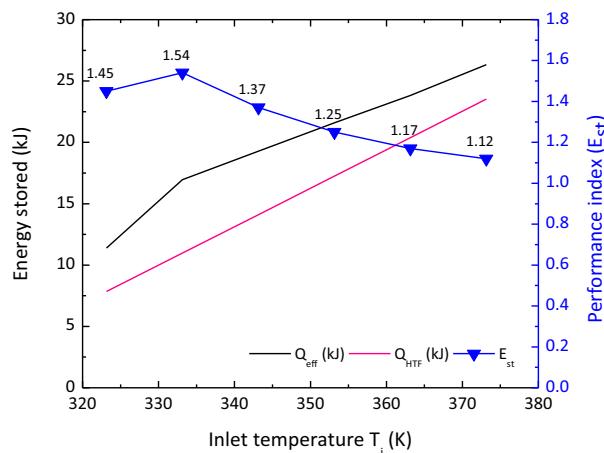
Fig. 15. Effect of inlet temperature (T_i) on stored energy and performance index.

Q_{eff} gradually decreases with increasing $\dot{V}$ and with this, drop in performance index E_{st} happens. As HTF mass flow rate increases with increasing $\dot{V}$, the time for reaching T_{out} reduces and its yields into dropping E_{st}. The performance index $E_{st} > 1$ for $\dot{V} < 300$ l/min, indicating the effective TES system. Therefore, a lower volumetric flow rate makes the TES system effective.

3.5. Variation of inlet temperature (T_i)

The HTF inlet temperature T_i from 323.15 K to 393.15 K, it was chosen to inspect its impact on the performance index. The tube diameter and length were set as $d = 10$ mm and $L = 5$ m. The volumetric flow rate $\dot{V}$ and initial temperature T_o were 20 l/min and 298.15 K, respectively. The impact of inlet temperature T_i on energy stored and performance index is shown in Fig. 15. As observed, with increasing T_i, performance index E_{st} first increases and then declines. The improve in E_{st} was 6.2% due to increase Q_{eff}. Here, it is noted that the melting temperature was 322.25 K as the average value of solidus and liquidus temperatures (T_s and T_l). The lower T_i is 323.15 K which is close to the melting temperature. It means the melt fraction of PCM with a lower T_i close to melting point would be less compared to a higher T_i. The time when T_{out} reach the specific value, only 57% of PCM was melted for $T_i = 323.15$ K and obvious, HTF and PCM exchanged less amount of heat. The performance index E_{st} of 1.54 was maximum for T_i 333.15 K. Further increase in T_i leads to drop in E_{st}. It should be noted that as T_i increases, outlet temperature T_{out} also increased to keep the minimum effectiveness η of 0.8. Therefore, Q_{eff} and Q_{HTF} increase due to increasing temperature differences (T_i-T_{out}) and (T_i-T_o), respectively, but Q_{HTF} dominates with increase T_i and yielded in lowering the ratio of Q_{eff} and Q_{HTF}. As a result, drop in E_{st} took place with increasing T_i.

3.6. Comparison with other existing work

In this work, the performance evaluation was performed for the present TES system where pure PCM ($k = 0.2$ W/m.K) was used. Very few works were reported in assessing the performance of PCM-based TES systems, where the variation of effective thermal conductivity and length-to-diameter ratio (L/d) was conducted [35,36,54]. The pure PCM, or thermal conductivity closer to 0.2 W/m.K, has been chosen from the literature to compare the performance of the present model. As the current configuration has a low L/d ratio, L/d up to 1000 was considered from Liang et al. [36] for the sake of comparison. The comparison results are indicated in Table 6. The performance index in the present study is comparably good with other reported works at given thermal conductivity.

4. Conclusions

This work presented numerical investigations of heat transfer concerning the influence of design parameters and operating conditions for shell-and-tube TES, in which the PCM was packed in the tube. A three-dimensional cyclic periodic model was performed to estimate the performance index of the shell-and-tube TES system for varying geometrical parameters, including diameter d and length L, and operating parameters, i.e., initial temperature T_o, inlet temperature T_i, and volumetric flow rate $\dot{V}$. In the different conditions, the effective energy storage ratio E_{st} was evaluated based on the effectiveness-NTU theory. The study of geometrical parameters on effective energy storage ratio E_{st} revealed that tubes with longer lengths and smaller diameters performed well. The geometrical parameters for which TES was effective were $d \leq 30$ mm and $L \geq 2$ m. The maximum PCM volume ratio V_r of 0.8 was obtained for the TES, which was effective. Beyond a specific value of V_r, the heat was wasted as HTF was going out of the tube directly rather than exchanging it with PCM. Next, the effective heat transfer was observed for the lower initial temperature T_o and noticed to be an effective TES up to $T_o < 301$ K. Further, the TES system was effective for the volumetric flow rate $\dot{V} < 300$ l/min. In the last, it was noticed that performance index E_{st} first increased slightly and then decreased with increasing inlet temperature T_i. The performance of 1.54 was achieved as a maximum for $T_i = 333.15$ K. The present TES model with pure PCM ($k = 0.2$ W/m. K) was compared with other models reported in the literature, and the current model performed comparatively well with other models. The present study could help design a low-temperature TES system for space heating applications. Moreover, investigations for different effective thermal conductivity and optimization are extended as part of our future work.

Nomenclature

A	Area of HTF cross-section, m^2
A_m	Mushy zone constant
c_p	Specific heat capacity, J/kg·K
D	Diameter of tank, m
d	Tube diameter, mm
d_h	Hydraulic diameter, m
E_{st}	Performance index

Table 6
Comparison of the performance index with other works.

Source	PCM	Thermal conductivity (W/m·K)	Outcomes
Fang et al. [35]	Tetradecane and hexadecane binary mixtures	0.14	The performance index was 0.59.
Liang et al. [36]	Tetradecane and hexadecane binary mixtures	0.14	The performance index was 1.3
Fang et al. [54]	PCM-EG composites	1	The performance index was 0.83.
Present study	Paraffin wax (RT 50)	0.2	The performance index is 1.54.

$\vec{g}$	Gravity, m/s^2
h_s	Sensible enthalpy, kJ/kg
h_{ref}	Reference enthalpy, kJ/kg
ΔH	Latent heat content, kJ/kg
H	Total enthalpy, kJ/kg
k	Thermal conductivity, W/m·K
L	Length of tube, m
L_h	Latent heat of PCM, kJ/kg
$\dot{m}$	Mass flow rate, kg/s
n_t	Required number of tubes
p	Pressure, N/m^2
P	Perimeter, m
Q_{eff}	Effective energy storage capacity, kJ
Q_{HTF}	Effective energy storage capacity of the conventional system, kJ
Q_{pump}	Energy consumption by pump, kJ
Q_∞	Theoretical energy storage capacity, kJ
Re	Reynolds number
$\vec{S}$	Source term
t_c	Tube thickness, mm
t	Time, s
t_{eff}	Effective time, s
T_o	Initial temperature, K
T_i	Inlet temperature, K
T_{out}	Outlet temperature, K
T_c	Cut-off temperature, K
T_m	Melting temperature, K
T_s	Solidus temperature, K
T_l	Liquidus temperature, K
u_i	Inlet velocity, m/s
$\bar{u}$	Average velocity, m/s
V	Volume, m^3
$\vec{V}$	Velocity vector, m/s
$\dot{V}$	Volumetric flow rate, l/min
V_r	PCM volume ratio
y	Axial distance, m
z	Radial distance, mm

Greek symbols

ρ	Density, kg/m^3
μ	Viscosity, kg/m·s

η	Effectiveness
η_{cycle}	Energy payback cycle
β	Thermal expansion coefficient, 1/K
λ	Melt fraction

Abbreviations

HTF	Heat transfer fluid
HX	Heat exchanger
NTU	Number of transfer units
PCM	Phase change material
TES	Thermal energy storage

CRediT authorship contribution statement

Abhinav Rajan: Writing – original draft, Visualization, Validation, Software, Methodology, Investigation, Formal analysis, Data curation. **Yixiang Gan:** Supervision, Methodology. **K.S. Reddy:** Writing – review & editing, Visualization, Supervision, Resources, Project administration, Methodology, Investigation, Formal analysis, Conceptualization.

Declaration of competing interest

The authors declare that they have no known competing financial interests or personal relationships that could have appeared to influence the work reported in this paper.

Data availability

Data will be made available on request.

Appendix

A.1. Calculation of inlet velocity u_i

The circle packing number n_t, i.e., the number of tubes in TES can be estimated from the tank to hexagon cross-section ratio.

$$n_t = \frac{\frac{\pi D^2}{4}}{\frac{6d^2}{4\sqrt{3}}} = \frac{\sqrt{3}\pi}{6}\frac{D^2}{d^2} \tag{A.1}$$

where D and d are the diameters of the TES tank and PCM-packed cylindrical tube, respectively.

The inlet flow velocity u_i and Reynolds number Re for HTF can be determined from the given volumetric flow rate $\dot{V}$ of the TES system.

$$u_i = \frac{\dot{V}}{n_t A} \tag{A.2}$$

where A is the HTF flow area (annulus region).

$$Re = \frac{\rho_w u_i d_h}{\mu_w} \tag{A.3}$$

where ρ_w and μ_w are density and viscosity of HTF, and d_h is the hydraulic diameter for the HTF section.

$$d_h = \frac{4A}{P} \tag{A.4}$$

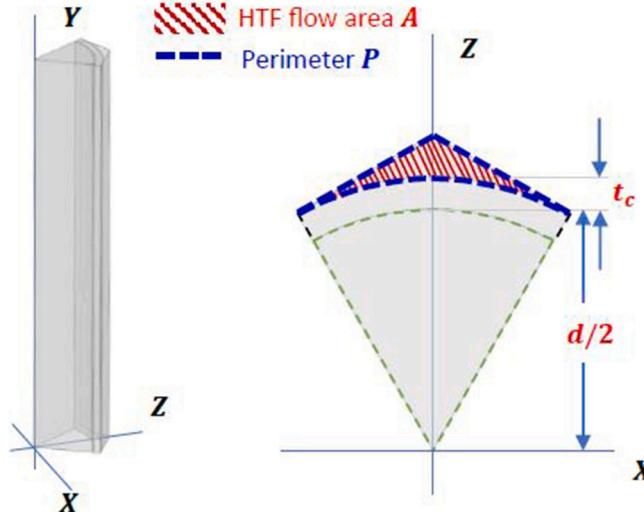where, P is the perimeter of the HTF inlet section, as shown in Fig. A.1.

Fig. A.1. Outline of one-sixth (1/6) of the hexagonal domain.

A.2. Effect of tube thickness

The tube length and diameter were fixed at 2 m and 20 mm, respectively, to investigate the influence of tube thickness t_c on the performance index E_{st}. The tube thickness t_c was chosen from 0.25 mm to 1.50 mm. The effects of tube thickness t_c are shown in Table A.2.
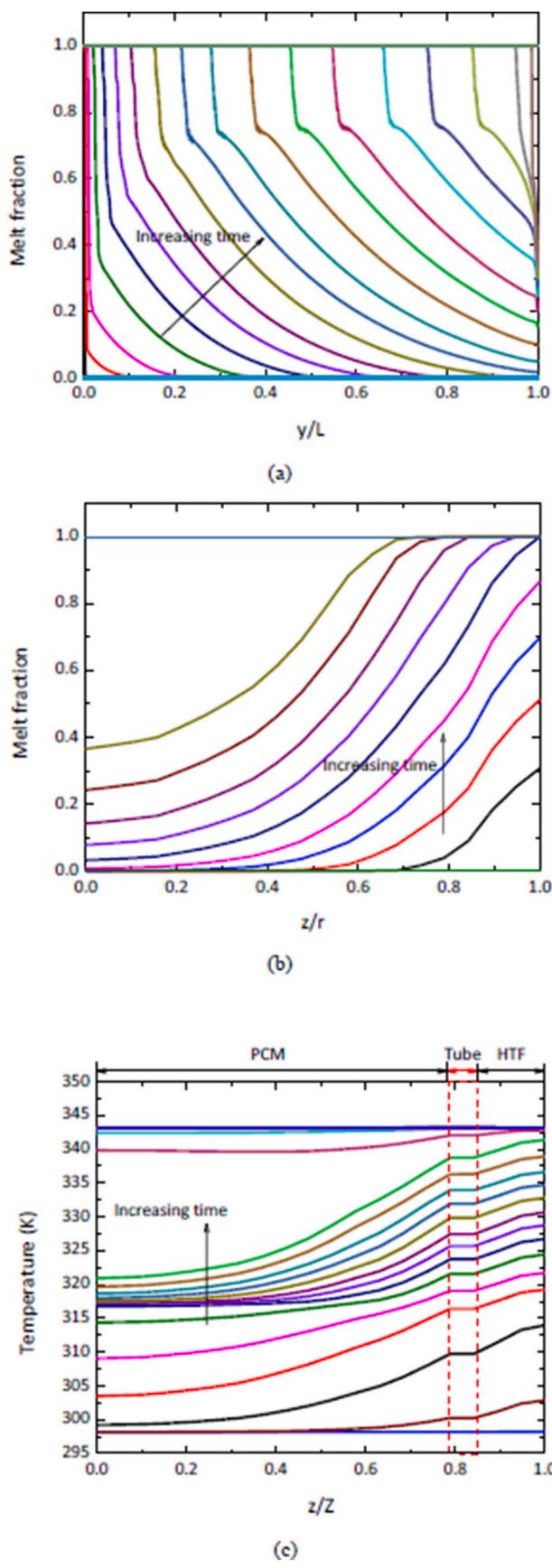
Table A.2
Impact of tube thickness t_c.

Thickness t_c (mm)	Q_{eff} (kJ)	Q_{HTF} (kJ)	E_{st}	Deviation $= \frac{E_{st}^j - E_{st}^{j-1}}{E_{st}^{j-1}} \times 100$ (%)
0.25	21.46	21.79	0.98	–
0.50	22.14	21.90	1.01	3.06
1.00	22.71	22.12	1.03	1.98
1.50	24.12	22.34	1.08	4.85

A.3. Melt fraction and temperature distributions

The melt fraction profile in the axial and radial directions and the radial temperature distribution are provided in Fig. A.2(a–c) for a better understanding of the melting process.

Fig. A.2. Melt and temperature distributions (a) melt fraction of PCM in the axial direction, (b) melt fraction of PCM in the radial direction at $y = L/2$, and (c) temperature distribution in the radial direction at $y = L/2$.

References

[1] R.Q. Wang, L. Jiang, Y.D. Wang, A.P. Roskilly, Energy saving technologies and mass-thermal network optimization for decarbonized iron and steel industry: a review, J. Clean. Prod. 274 (2020) 122997, https://doi.org/10.1016/J.JCLEPRO.2020.122997.

[2] Y. Tian, C.Y. Zhao, A review of solar collectors and thermal energy storage in solar thermal applications, Appl. Energy 104 (2013) 538–553, https://doi.org/10.1016/J.APENERGY.2012.11.051.

[3] N. Soni, D. Sharma, M.M. Rahman, P.R. Hanmaiahgari, V.M. Reddy, Mathematical modeling of solar energy based thermal energy storage for house heating in winter, J. Energy Storage. 34 (2021) 102203, https://doi.org/10.1016/j.est.2020.102203.

[4] N. Pradeep, K.S. Reddy, Design and investigation of solar cogeneration system with packed bed thermal energy storage for ceramic industry, Renew. Energy 192 (2022) 243–263, https://doi.org/10.1016/J.RENENE.2022.04.087.

[5] Y. Qin, M. Ghalambaz, M. Sheremet, M. Fteiti, F. Alresheedi, A bibliometrics study of phase change materials (PCMs), J. Energy Storage. 73 (2023) 108987, https://doi.org/10.1016/j.est.2023.108987.

[6] A.K. Ray, D. Rakshit, K. Ravikumar, High-temperature latent thermal storage system for solar power: materials, concepts, and challenges, Clean. Eng. Technol. 4 (2021) 100155, https://doi.org/10.1016/J.CLET.2021.100155.

[7] J. Sunku Prasad, P. Muthukumar, F. Desai, D.N. Basu, M.M. Rahman, A critical review of high-temperature reversible thermochemical energy storage systems, Appl. Energy 254 (2019) 113733, https://doi.org/10.1016/J.APENERGY.2019.113733.

[8] F. Agyenim, N. Hewitt, P. Eames, M. Smyth, A review of materials, heat transfer and phase change problem formulation for latent heat thermal energy storage systems (LHTESS), Renew. Sust. Energ. Rev. 14 (2010) 615–628, https://doi.org/10.1016/j.rser.2009.10.015.

[9] M. Esen, A. Durmuş, A. Durmuş, Geometric design of solar-aided latent heat store depending on various parameters and phase change materials, Sol. Energy 62 (1998) 19–28, https://doi.org/10.1016/S0038-092X(97)00104-7.

[10] N.R. Vyshak, G. Jilani, Numerical analysis of latent heat thermal energy storage system, Energy Convers. Manag. 48 (2007) 2161–2168, https://doi.org/10.1016/J.ENCONMAN.2006.12.013.

[11] M. Akgün, O. Aydin, K. Kaygusuz, Experimental study on melting/solidification characteristics of a paraffin as PCM, Energy Convers. Manag. 48 (2007) 669–678, https://doi.org/10.1016/J.ENCONMAN.2006.05.014.

[12] S. Seddegh, X. Wang, A.D. Henderson, A comparative study of thermal behaviour of a horizontal and vertical shell-and-tube energy storage using phase change materials, Appl. Therm. Eng. 93 (2016) 348–358, https://doi.org/10.1016/j.applthermaleng.2015.09.107.

[13] S. Jain, K. Ravi Kumar, D. Rakshit, B. Premachandran, K.S. Reddy, Influence of the storage orientation and shell shape on the melting dynamics of shell and tube-type cascade latent heat storage, Appl. Therm. Eng. 231 (2023) 120923, https://doi.org/10.1016/j.applthermaleng.2023.120923.

[14] Y.Q. Li, Y.L. He, H.J. Song, C. Xu, W.W. Wang, Numerical analysis and parameters optimization of shell-and-tube heat storage unit using three phase change materials, Renew. Energy 59 (2013) 92–99, https://doi.org/10.1016/J.RENENE.2013.03.022.

[15] W. Youssef, Y.T. Ge, S.A. Tassou, CFD modelling development and experimental validation of a phase change material (PCM) heat exchanger with spiral-wired tubes, Energy Convers. Manag. 157 (2018) 498–510, https://doi.org/10.1016/J.ENCONMAN.2017.12.036.

[16] M. Lacroix, Numerical simulation of a shell-and-tube latent heat thermal energy storage unit, Sol. Energy 50 (1993) 357–367, https://doi.org/10.1016/0038-092X(93)90029-N.

[17] M. Samykano, Role of phase change materials in thermal energy storage: potential, recent progress and technical challenges, Sustain. Energy Technol. Assessments. 52 (2022) 102234, https://doi.org/10.1016/j.seta.2022.102234.

[18] A. Mills, M. Farid, J.R. Selman, S. Al-Hallaj, Thermal conductivity enhancement of phase change materials using a graphite matrix, Appl. Therm. Eng. 26 (2006) 1652–1661, https://doi.org/10.1016/J.APPLTHERMALENG.2005.11.022.

[19] C. Wang, K. Chen, J. Huang, Z. Cai, Z. Hu, T. Wang, Thermal behavior of polyethylene glycol based phase change materials for thermal energy storage with multiwall carbon nanotubes additives, Energy 180 (2019) 873–880, https://doi.org/10.1016/J.ENERGY.2019.05.163.

[20] Z. Li, Z.G. Wu, Numerical study on the thermal behavior of phase change materials (PCMs) embedded in porous metal matrix, Sol. Energy 99 (2014) 172–184, https://doi.org/10.1016/J.SOLENER.2013.11.017.

[21] L. Kalapala, J.K. Devanuri, Influence of operational and design parameters on the performance of a PCM based heat exchanger for thermal energy storage – a review, J. Energy Storage. 20 (2018) 497–519, https://doi.org/10.1016/j.est.2018.10.024.

[22] M.K. Rathod, J. Banerjee, Thermal performance enhancement of shell and tube Latent Heat Storage Unit using longitudinal fins, Appl. Therm. Eng. 75 (2015) 1084–1092, https://doi.org/10.1016/j.applthermaleng.2014.10.074.

[23] K.A. Aly, A.R. El-Lathy, M.A. Fouad, Enhancement of solidification rate of latent heat thermal energy storage using corrugated fins, J. Energy Storage. 24 (2019) 100785, https://doi.org/10.1016/J.EST.2019.100785.

[24] H. Masoumi, R. Haghighi Khoshkhoo, S.M. Mirfendereski, Experimental and numerical investigation of melting/solidification of nano-enhanced phase change materials in shell & tube thermal energy storage systems, J. Energy Storage. 47 (2022) 103561, https://doi.org/10.1016/J.EST.2021.103561.

[25] Y. Zhang, A. Faghri, Heat transfer enhancement in latent heat thermal energy storage system by using the internally finned tube, Int. J. Heat Mass Transf. 39 (1996) 3165–3173, https://doi.org/10.1016/0017-9310(95)00402-5.

[26] A. Vikas, S. Yadav, Samir, Melting dynamics analysis of a multi-tube latent heat thermal energy storage system: numerical study, Appl. Therm. Eng. 214 (2022) 118803, https://doi.org/10.1016/j.applthermaleng.2022.118803.

[27] V. Safari, B. Kamkari, H. Abolghasemi, Investigation of the effects of shell geometry and tube eccentricity on thermal energy storage in shell and tube heat exchangers, J. Energy Storage. 52 (2022) 104978, https://doi.org/10.1016/j.est.2022.104978.

[28] J.R. Patel, M.K. Rathod, M. Sheremet, Heat transfer augmentation of triplex type latent heat thermal energy storage using combined eccentricity and longitudinal fin, J. Energy Storage. 50 (2022) 104167, https://doi.org/10.1016/J.EST.2022.104167.

[29] R.P. Singh, S.C. Kaushik, D. Rakshit, Melting phenomenon in a finned thermal storage system with graphene nano-plates for medium temperature applications, Energy Convers. Manag. 163 (2018) 86–99, https://doi.org/10.1016/J.ENCONMAN.2018.02.053.

[30] A.M. Abdulateef, J. Abdulateef, A.A. Al-Abidi, K. Sopian, S. Mat, M.S. Mahdi, A combination of fins-nanoparticle for enhancing the discharging of phase-change material used for liquid desiccant air conditioning unite, J. Energy Storage. 24 (2019) 100784, https://doi.org/10.1016/J.EST.2019.100784.

[31] S. Zhang, Y. Yan, Y. Jin, Y. Gao, Comprehensive thermal energy storage analysis of ceramic foam-enhanced molten salt in a shell-and-tube unit, Sol. Energy 255 (2023) 381–395, https://doi.org/10.1016/j.solener.2023.02.021.

[32] S. Jain, K.R. Kumar, D. Rakshit, B. Premachandran, K.S. Reddy, Cyclic performance assessment of medium-temperature cascade thermal energy storage, J. Energy Storage. 68 (2023) 107662, https://doi.org/10.1016/j.est.2023.107662.

[33] N. Soni, V.M. Reddy, K.S. Reddy, Modeling and analysis of PCM-encapsulated solar thermal energy storage system for space heating, Energy Storage. (2023) 1–19, https://doi.org/10.1002/est2.537.

[34] W.W. Wang, L.B. Wang, Y.L. He, The energy efficiency ratio of heat storage in one shell-and-one tube phase change thermal energy storage unit, Appl. Energy 138 (2015) 169–182, https://doi.org/10.1016/j.apenergy.2014.10.064.

[35] Y. Fang, J. Niu, S. Deng, Numerical analysis for maximizing effective energy storage capacity of thermal energy storage systems by enhancing heat transfer in PCM, Energ. Buildings 160 (2018) 10–18, https://doi.org/10.1016/j.enbuild.2017.12.006.

[36] H. Liang, J. Niu, Y. Gan, Performance optimization for shell-and-tube PCM thermal energy storage, J. Energy Storage. 30 (2020) 101421, https://doi.org/10.1016/j.est.2020.101421.

[37] N.A.M. Amin, M. Belusko, F. Bruno, M. Liu, Optimising PCM thermal storage systems for maximum energy storage effectiveness, Sol. Energy 86 (2012) 2263–2272, https://doi.org/10.1016/J.SOLENER.2012.04.020.

[38] H. El Qarnia, Numerical analysis of a coupled solar collector latent heat storage unit using various phase change materials for heating the water, Energy Convers. Manag. 50 (2009) 247–254, https://doi.org/10.1016/J.ENCONMAN.2008.09.038.

[39] E. Talmatsky, A. Kribus, PCM storage for solar DHW: an unfulfilled promise? Sol. Energy 82 (2008) 861–869, https://doi.org/10.1016/J.SOLENER.2008.04.003.

[40] T. Yang, W.P. King, N. Miljkovic, Phase change material-based thermal energy storage, Cell Reports Phys. Sci. 2 (2021) 100540, https://doi.org/10.1016/j.xcrp.2021.100540.

[41] A. Rajan, K.S. Reddy, Integrated optical and thermal model to investigate the performance of a solar parabolic dish collector coupled with a cavity receiver, Renew. Energy 219 (2023) 119376, https://doi.org/10.1016/j.renene.2023.119376.

[42] A. Rajan, K.S. Reddy, Integrated optical-thermal model and deep learning technique to estimate the performance of a conical cavity receiver coupled solar parabolic dish collector, Energy Convers. Manag. 301 (2024) 118052, https://doi.org/10.1016/j.enconman.2023.118052.

[43] H. Liang, J. Niu, R.K. Annabattula, K.S. Reddy, A. Abbas, M.T. Luu, Y. Gan, Phase change material thermal energy storage design of packed bed units, J. Energy Storage. 51 (2022) 104576, https://doi.org/10.1016/j.est.2022.104576.

[44] T.L.Bergman, L. A.S, I. F.P., D.P. DeWitt, Fundamentals of Heat and Mass Transfer, 7th editio, John Wiley & Sons Seventh, 2011.

[45] M. Ismail, A.H. Alkhazaleh, J. Masri, A.M. Ali, M. Ali, Experimental and numerical analysis of paraffin waxes during solidification inside spherical capsules, Therm. Sci. Eng. Prog. 26 (2021) 101095, https://doi.org/10.1016/j.tsep.2021.101095.

[46] M.J. Hosseini, M. Rahimi, R. Bahrampoury, Experimental and computational evolution of a shell and tube heat exchanger as a PCM thermal storage system, Int. Commun. Heat Mass Transf. 50 (2014) 128–136, https://doi.org/10.1016/j.icheatmasstransfer.2013.11.008.

[47] K.S. Reddy, S. Balaji, T. Sundararajan, Estimation of heat losses due to wind effects from linear parabolic secondary reflector –receiver of solar LFR module, Energy 150 (2018) 410–433, https://doi.org/10.1016/j.energy.2018.02.125.

[48] H. Soltani, M. Soltani, H. Karimi, J. Nathwani, Optimization of shell and tube thermal energy storage unit based on the effects of adding fins, nanoparticles and rotational mechanism, J. Clean. Prod. 331 (2022) 129922, https://doi.org/10.1016/j.jclepro.2021.129922.

[49] ANSYS Fluent Theory Guide, 20R1, ANSYS Inc, USA. https://www.ansys.com/products/fluids/ansys-fluent. (n.d.).

[50] G. Alva, Y. Lin, G. Fang, An overview of thermal energy storage systems, Energy 144 (2018) 341–378, https://doi.org/10.1016/J.ENERGY.2017.12.037.

[51] D. Paul, C. Ionescu, H. Necula, Study of thermal energy storage using phase change materials, in: 2017 Int. Conf. Energy Environ, IEEE, 2017, pp. 162–166, https://doi.org/10.1109/CIEM.2017.8120763.

[52] A.T. Fox, R. W., and McDonald, Fox and McDonald's Introduction to Fluid Mechanics, 8th Edition - Philip J. Pritchard, 1999. https://www.mendeley.com/catalogue/38fda33e-816b-3841-880e-a1a4994500a2/ (accessed August 26, 2023).

[53] P.G. Hammond, C. Jones, Inventory of Carbon & Energy (ICE) ICE (Inventory of Carbon & Energy), Mech. Eng. www.bath.ac.uk/mech-eng/sert/embodied/, 2006. (Accessed 26 August 2023).

[54] Y. Fang, H. Xu, Y. Miao, Z. Bai, J. Niu, S. Deng, Experimental study of storage capacity and discharging rate of latent heat thermal energy storage units, Appl. Energy 275 (2020) 115325, https://doi.org/10.1016/j.apenergy.2020.115325.